Check for updates

Modulation of 2-imino-6,7-dihydroquinlin-8(5*H*)-imine-iron ethylene polymerization catalysts through (cyclo)alkyl, benzhydryl and halide substitution

Randi Zhang,[ab] Yanping Ma, [iD][b] Gregory A. Solan,*[bc] Yizhou Wang,[b] Jiahao Gao,[b] Tongling Liang [iD][b] and Wen-Hua Sun [iD]*[b]

A direct one-pot assembly has been utilized for the preparation of 2-imino-6,7-dihydroquinlin-8(5*H*)-imine-ferrous chloride complexes, [2-(ArN=CCH₃)-8-(ArN)C₉H₈N]FeCl₂ (Ar = 2-Me-4-(CHPh₂)-6-(C₅H₉)C₆H₂ **Fe1**, 2-Me-4-(C₅H₉)-6-(CHPh₂)C₆H₂ **Fe2**, 2-(C₅H₉)-4-Me-6-(CHPh₂)C₆H₂ **Fe3**, 2-(C₅H₉)-4,6-(CHPh₂)₂C₆H₂ **Fe4**, 2-(C₆H₁₁)-4,6-(CHPh₂)₂C₆H₂ **Fe5**, 2-(C₈H₁₅)-4,6-(CHPh₂)₂C₆H₂ **Fe6**, 2-F-4,6-(CHPh₂)₂C₆H₂ **Fe7**, 2-Cl-4,6-(CHPh₂)₂C₆H₂ **Fe8**], disparate in the steric/electronic profile of their *N*-aryl groups. In addition to spectroscopic characterization, the structural properties of representative **Fe3** and **Fe5** have been determined by single crystal XRD. Under activation with MAO or MMAO, **Fe1–Fe8** displayed very high catalytic activities for ethylene polymerization at 60 °C [up to 25.20×10^6 g (PE) per mol (Fe) per h for **Fe2**/MMAO]; even at temperatures as high as 100 °C the activity remained high [3.92×10^6 g (PE) per mol (Fe) per h]. Notably, the polymers generated using MMAO as activator showed distinctly lower molecular weight than those with MAO [M_w range: 1.36–62.41 kg mol^{-1} (MMAO) *vs.* 13.07–210.56 kg mol^{-1} (MAO)], with *ortho*-cycloalkyl-containing **Fe4–Fe6** forming polymers at the lowest end of the M_w range and with the narrowest dispersity (M_w/M_n range: 1.6–2.3). Microstructural analysis of selected polymers highlighted the presence of both vinyl-terminated polymers and fully saturated polymers, the ratio of which could be influenced by not only the type of aluminum-alkyl activator but also by the run temperature and the *N*-aryl substitution pattern. Significantly, the molecular weights of many of these polyethylenes fall within the specification range for polyethylene waxes used in industrial applications.

Introduction

Divalent metal halide complexes of the late first row *d*-block metals such as cobalt and iron have been at the forefront of homogeneous catalysis research for close to three decades due, in good measure, to their use as precatalysts for the polymerization of ethylene.[1,2] Indeed, the discovery that the 2,6-bis(imino)pyridine ligand frame can provide an effective support for the polymerization-active iron and cobalt metal centers has provided the motivation for a raft of reports and reviews (**A**, Chart 1).[3,4] This can in part be attributed to the amenability of this ligand frame to systematic modification in its substitution

pattern thereby allowing a means to tune polymerization performance in terms of catalytic activity and optimum run temperature range, as well as regulating properties of the resulting polymers.[5] More recent developments have seen alternative *N,N,N*-ligand sets emerge, in particular those based on carbocyclic-fused bis(imino)pyridines that can be distinguished by their fused ring size (**B–D**, Chart 1). Such modifications can not only improve the activity and thermal stability of the iron or cobalt catalyst, but also impart significant effects on the polymer products and catalytic activity.[6–11]

Hitherto, both singly[7,8] and doubly[6,9–11] fused examples of metal complexes have been reported with carbocyclic ring sizes ranging from six to eight. With particular regard to iron, both doubly fused **B₇,₇** ($n = 2$)[10] and singly fused **C₆** ($n = 1$),[7] can display very high catalytic activities (up to 2.5×10^7 g PE per mol (Fe) per h, **B₇,₇** (ref. 10*b*)) and good thermal stability affording polyethylenes with significant levels of vinyl end-groups. Moreover, correlations have emerged between the properties of the resulting polymeric material and the fused ring size. Elsewhere, regulation of steric hindrance of the substituents

ᵃSINOPEC (Beijing) Research Institute of Chemical Industry Co., Ltd, No. 14 Beisanhuan Donglu, Chao Yang District, Beijing 100013, China. E-mail: zhangrd.bjhy@sinopec.com

ᵇKey Laboratory of Engineering Plastics and Beijing National Laboratory for Molecular Sciences, Institute of Chemistry, Chinese Academy of Sciences, Beijing 100190, China. E-mail: whsun@iccas.ac.cn; Tel: +86-10-62557955

ᶜDepartment of Chemistry, University of Leicester, University Road, Leicester LE1 7RH, UK. E-mail: gas8@leicester.ac.uk; Tel: +44-116 2522096
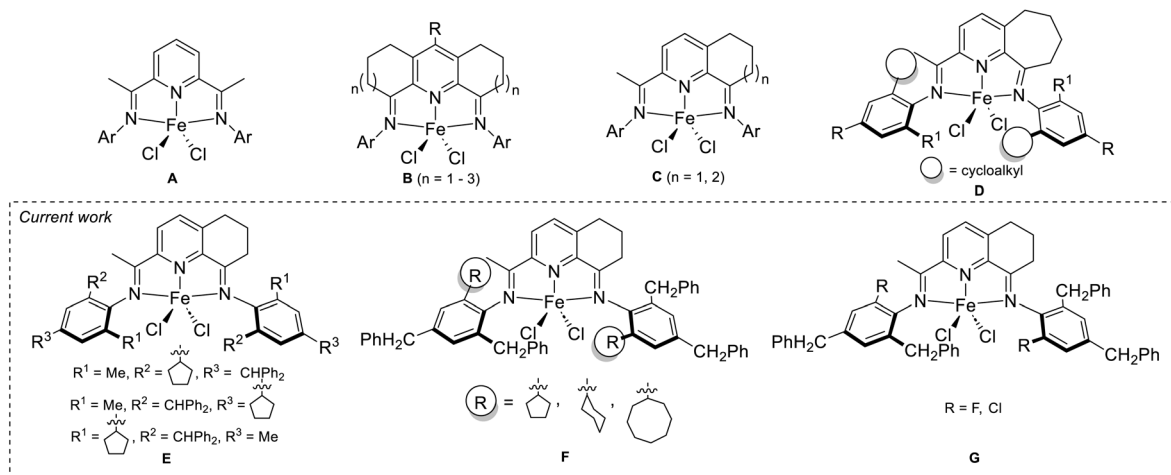
Chart 1 Bis(imino)pyridine-containing **A**, its carbocyclic-fused derivatives **B–D**, and the 2-imino-6,7-dihydroquinlin-8(5H)-imine systems to be investigated in this work, **E**, **F** and **G**.

within the fused ligand frame has also been the subject of a number of studies. For example, the *ortho*-cycloalkyl substituted iron precatalyst $\mathbf{D}_{R/R1=Me}$[8b] showed its optimal activity at 80 °C [as high as 1.9×10^7 g of PE per mol (Fe) per h], while substitution of the *ortho*/*para*-methyl groups in $\mathbf{D}_{R/R1=Me}$ with "super-bulky" benzhydryl groups (CHPh$_2$) as in $\mathbf{D}_{R/R1=CHPh_2}$,[8c] afforded polyethylene waxes with high molecular weights (up to 55.6 kg mol^{-1}).
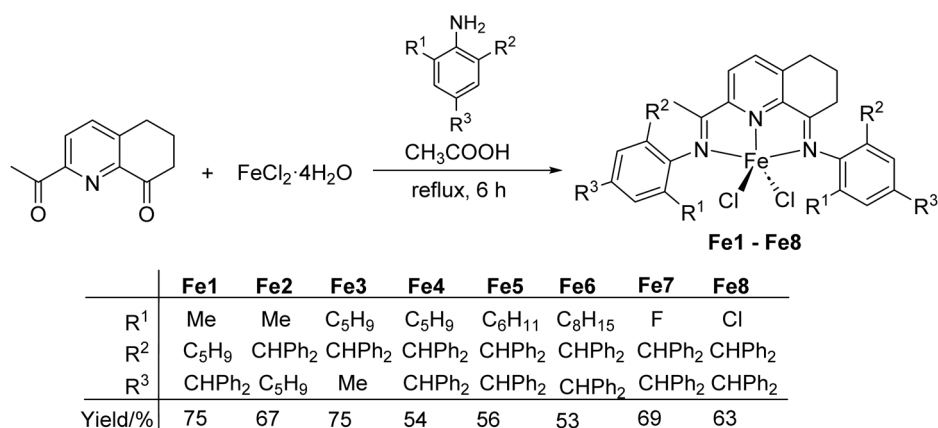
With the aim to gain a deeper understanding of the effect of combining both (cyclo)alkyl and benzhydryl as part of the *N*-aryl substitution pattern, we returned our attention to the singly-fused framework **C** ($n = 1$, Chart 1) so as to systematically explore how the positioning and type of this group impact on catalytic performance, thermal stability and polymer properties. To broaden the range of *ortho*-substituents, we also extend the study to include the effect of electron withdrawing halide substituents. Accordingly, three sub-classes of 2-imino-6,7-di-hydroquinlin-8(5H)-imine-iron(II) chloride precatalyst are tar-geted, **E**, **F** and **G** (Chart 1), in which **E** contains three permutations of benzhydryl, cyclopentyl and methyl in the

2,4,6-positions, **F** contains three distinct ring sizes for the *ortho*-cycloalkyl groups and **G** differs in the electronic properties of the *ortho*-halide substituent (fluoride *vs.* chloride). A comprehensive investigation of all three sub-classes of iron precatalyst for ethylene polymerization is then conducted with two types of aluminum-alkyl activator that explores modifications to the temperature, pressure and run time; thorough comparisons are then made between catalysts developed in the work and with literature examples. Besides an in-depth study of various properties of the resulting polyethylenes, all new iron complexes are fully characterized. Our findings regarding the cobalt derivatives of **E**, **F** and **G** have recently been disclosed.[12]

Results and discussion

Synthesis and characterization of the iron precatalysts

The 2-imino-6,7-dihydroquinlin-8(5H)-imine-iron(II) chloride complexes, [2-(ArN=CCH$_3$)-8-(ArN)C$_9$H$_8$N]FeCl$_2$ (Ar = 2-Me-4-(CHPh$_2$)-6-(C$_5$H$_9$)C$_6$H$_2$ **Fe1**, 2-Me-4-(C$_5$H$_9$)-6-(CHPh$_2$)C$_6$H$_2$ **Fe2**, 2-(C$_5$H$_9$)-4-Me-6-(CHPh$_2$)C$_6$H$_2$ **Fe3**, 2-(C$_5$H$_9$)-4,6-(CHPh$_2$)$_2$C$_6$H$_2$

Scheme 1 One-pot assembly of **Fe1–Fe8**.

	Fe1	Fe2	Fe3	Fe4	Fe5	Fe6	Fe7	Fe8
R^1	Me	Me	C$_5$H$_9$	C$_5$H$_9$	C$_6$H$_{11}$	C$_8$H$_{15}$	F	Cl
R^2	C$_5$H$_9$	CHPh$_2$	CHPh$_2$	CHPh$_2$	CHPh$_2$	CHPh$_2$	CHPh$_2$	CHPh$_2$
R^3	CHPh$_2$	C$_5$H$_9$	Me	CHPh$_2$	CHPh$_2$	CHPh$_2$	CHPh$_2$	CHPh$_2$
Yield/%	75	67	75	54	56	53	69	63

© 2025 The Author(s). Published by the Royal Society of Chemistry

Fe4, 2-(C$_6$H$_{11}$)-4,6-(CHPh$_2$)$_2$C$_6$H$_2$ **Fe5**, 2-(C$_8$H$_{15}$)-4,6-(CHPh$_2$)$_2$-C$_6$H$_2$ **Fe6**, 2-F-4,6-(CHPh$_2$)$_2$C$_6$H$_2$ **Fe7**, 2-Cl-4,6-(CHPh$_2$)$_2$C$_6$H$_2$ **Fe8**), have been synthesized using a straightforward one-pot route that makes use of a combined condensation and complexation of 2-acetyl-6,7-dihydroquinolin-8(5H)-one, iron(II) chloride and two equivalents of the corresponding aniline in acetic acid (Scheme 1). On work-up, **Fe1–Fe8** were isolated in relatively good yields (53–67%) as air and moisture stable blue powders. Attempts to form the corresponding free 2-imino-6,7-dihydroquinlin-8(5H)-imines proved unsuccessful instead forming intractable mixtures. Similar one-pot approaches have been described for the synthesis of previously reported iron and cobalt compounds.[10–12] All eight complexes have been characterized by FT-IR spectroscopy, elemental analysis and for **Fe3** and **Fe5**, additionally by single crystal X-ray diffraction.

Crystals of **Fe3** and **Fe5** of suitable quality for the X-ray determinations were grown by slow diffusion of *n*-heptane into a solution of the corresponding complex in dichloromethane at room temperature. Perspective views of each structure are shown in Fig. 1 and 2, with selected bond lengths and angles listed in Table 1. The structures of **Fe3** and **Fe5** are similar differing only in the *N*-aryl group substitution pattern (*viz.* 2-cyclopentyl-4-methyl-6-benzhydrylphenyl **Fe3**, 2-
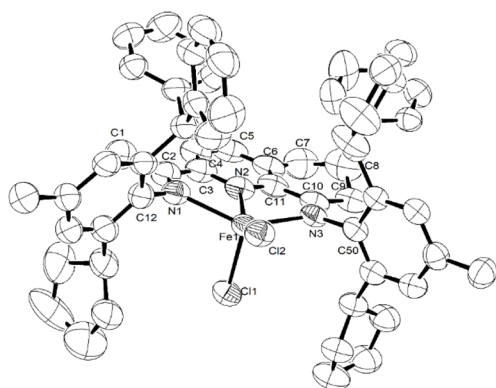
Table 1 Selected bond lengths (Å) and angles (°) for **Fe3** and **Fe5**

	Fe3	Fe5
Bond lengths (Å)		
Fe(1)–Cl(1)	2.3075(15)	2.2976(17)
Fe(1)–Cl(2)	2.2569(13)	2.2516(16)
Fe(1)–N(1)	2.241(5)	2.264(5)
Fe(1)–N(2)	2.074(4)	2.078(4)
Fe(1)–N(3)	2.229(4)	2.253(4)
N(1)–C(2)	1.294(7)	1.297(7)
N(1)–C(12)	1.436(7)	1.430(7)
N(2)–C(3)	1.357(8)	1.340(7)
N(2)–C(11)	1.339(7)	1.333(6)
N(3)–C(10)	1.293(6)	1.311(7)
N(3)–C(50)	1.443(6)	1.426(8)
Bond angles (°)		
Cl(1)–Fe(1)–Cl(2)	112.50(6)	114.10(7)
N(1)–Fe(1)–Cl(1)	100.59(11)	100.11(11)
N(1)–Fe(1)–Cl(2)	100.20(12)	99.62(12)
N(1)–Fe(1)–N(2)	73.80(18)	72.59(16)
N(1)–Fe(1)–N(3)	142.05(15)	142.26(16)
N(2)–Fe(1)–N(3)	72.81(17)	74.16(17)
N(2)–Fe(1)–Cl(1)	95.92(12)	99.92(12)
N(2)–Fe(1)–Cl(2)	151.58(12)	145.97(12)
N(3)–Fe(1)–Cl(1)	100.28(10)	102.73(12)
N(3)–Fe(1)–Cl(2)	100.56(10)	97.95(13)
C(8)–C(9)–C(10)	108.3(6)	110.7(6)
N(3)–C(10)–C(11)	115.1(5)	116.1(5)

Fig. 1 OLEX2 representation of **Fe3** with the thermal ellipsoids shown at the 50% probability level; all hydrogen atoms and solvents have been omitted for clarity.
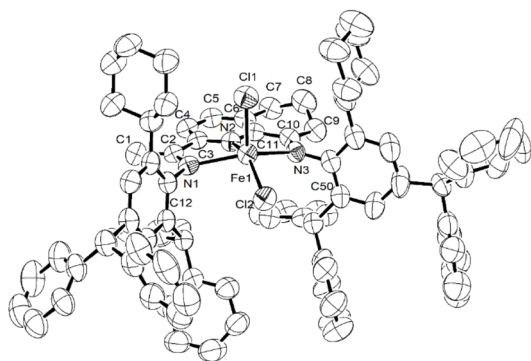

Fig. 2 OLEX2 representation of **Fe5** with the thermal ellipsoids shown at the 50% probability level; all hydrogen atoms and solvents have been omitted for clarity.

cyclohexyl-4,6-dibenzhydrylphenyl **Fe5**) and hence will be jointly described.

Each structure comprises a single iron(II) center bound by the three nitrogen donors belonging to the 2-imino-6,7-dihydroquinlin-8(5H)-imine and two chlorides to complete a five-coordinate geometry. Determination of the geometric tau value (τ_5) for each structure reveals values of 0.16 (**Fe3**) and 0.06 (**Fe5**), respectively, which are consistent with the geometrical description being referred to as distorted-square pyramidal.[3d] The three nitrogen atoms N(1), N(2) and N(3) and Cl(2) form the basal square plane while Cl(1) fills the apical position with the result that the iron atoms lie at a distance of 0.408 Å (**Fe3**) and 0.578 Å (**Fe5**) above the basal plane; similar observations have been seen in related *N,N,N*-iron(II) analogues.[7,8,10b,c] The central **Fe1**–N(2)$_{pyridine}$ bond distance in **Fe3** (2.074(4) Å) is comparable with that in **Fe5** (2.078(4) Å) but appreciably shorter than the exterior **Fe1**–N$_{imine}$ lengths (2.241(5) Å, 2.229(4) Å for **Fe3** and 2.264(5) Å, 2.253(4) Å for **Fe5**), highlighting the effective coordination of the central nitrogen donor. Minimal variation is seen in the imine N(1)–C(2) and N(3)–C(11) bond lengths and indeed typical of carbon nitrogen double bonds [1.294(7) Å *vs.* 1.293(6) Å for **Fe3**, 1.297(7) Å *vs.* 1.311(7) Å for **Fe5**]. In addition, the N(1)-aryl and N(3)-aryl ring planes in each structure are inclined towards perpendicular with respect to the *N,N,N*-coordination plane with dihedral angles of 69.53°/74.36° (**Fe3**) and 73.98°/71.36° (**Fe5**).[13] The modest differences between these two angles within each structure may reflect the steric variations between the *ortho*-cyclopentyl and *ortho*-cyclohexyl group. Moreover, the two cycloalkyl-substituents in each

structure are positioned on the same side of the coordination plane and *cis* with respect to the apical Cl(1), with the result that *ortho*-benzhydryl groups add steric protection below the basal plane.[8b,c,12] For both structures, the saturated section of two fused six-membered rings, C7–C8–C9, adopt the expected puckered configurations on account of the three sp^3-hybridized carbon atoms. No intermolecular contacts of note could be identified.

In terms of their spectroscopic properties, all eight complexes, **Fe1–Fe8**, exhibited absorption bands at 1602–1624 cm^{-1} in their IR spectra, wavenumbers that are characteristic of C=N stretching vibrations for iron-coordinated imines.[6–12] In addition, all ferrous complexes gave satisfactory microanalytical data for compositions based on N,N,N-FeCl$_2$.

Ethylene polymerization studies

Previous studies using iron precatalysts **A–F** (Chart 1) have identified that methylaluminoxane (MAO) and modified methylaluminoxane (MMAO; containing 20–25% Al(i-Bu)$_3$) are among the most suitable alkyl-aluminum activators to achieve optimum catalytic performance.[3,6–13] Hence, the current investigation focuses on these two activators as part of in-parallel studies. In order to ascertain the best set of conditions to screen **Fe1–Fe8**, **Fe5** was selected as the test precatalyst for each study, whereby variations in run temperature, Al : Fe molar ratio, run time and ethylene pressure are systematically varied (Tables 2–4). All resulting polymers are initially characterized by Gel Permeation Chromatography (GPC) to determine molecular
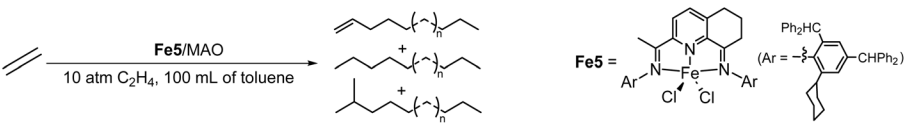
weight and dispersity, while differential scanning calorimetry (DSC) is used to measure melting temperatures. To check for oligomeric fractions, gas chromatography (GC) is additionally used in each case.

Table 3 Preliminary evaluation of **Fe5**/MAO for ethylene polymerization[a]

Entry	Al : Fe	t (min)	T (°C)	PE mass (g)	Activity[b]	M_w[c]	M_w/M_n[c]	T_m[d]
1	2000	30	30	2.41	2.41	120.97	17.12	135.9
2	2000	30	40	4.99	4.99	105.58	15.02	135.3
3	2000	30	50	3.10	3.10	104.77	10.25	135.2
4	2000	30	60	1.58	1.58	89.66	13.21	135.0
5	2000	30	70	0.41	0.41	80.49	14.02	134.2
6	1500	30	40	4.69	4.69	70.83	12.83	135.3
8	2500	30	40	6.01	6.01	94.07	12.14	134.3
9	3000	30	40	2.25	2.25	36.59	11.14	129.6
10	3500	30	40	0.92	0.92	36.37	12.46	129.5
11	2500	5	40	0.58	3.48	1.47	18.62	132.4
12	2500	15	40	2.36	4.72	78.10	22.15	135.0
13	2500	45	40	6.55	4.37	109.11	13.54	133.9
14	2500	60	40	7.22	3.61	133.11	13.78	134.8
15[e]	2500	30	40	0.92	0.92	48.56	3.20	135.0
16[f]	2500	30	40	Trace	—	—	—	—

[a] Conditions: 2.0 μmol of **Fe5**, 100 mL of toluene, 10 atm C$_2$H$_4$. [b] Values in units of 10^6 g (PE) per mol (Fe) per h. [c] M_w in units of kg mol^{-1}. M_w and M_w/M_n determined by GPC. [d] Determined by DSC. [e] 5 atm C$_2$H$_4$. [f] 1 atm C$_2$H$_4$.

Table 2 Preliminary evaluation of **Fe5**/MMAO for ethylene polymerization[a]

Entry	Al : Fe	t (min)	T (°C)	PE mass (g)	Activity[b]	M_w[c]	M_w/M_n[c]	T_m[d]
1	2000	30	30	4.47	4.47	11.92	2.18	127.0
2	2000	30	40	6.25	6.25	2.30	2.04	126.1
3	2000	30	50	7.76	7.76	1.67	1.72	126.0
4	2000	30	60	9.38	9.38	1.47	1.97	125.0
5	2000	30	70	1.62	1.62	0.98	1.52	123.2
6	2000	30	80	0.57	0.57	0.55	1.66	122.5
8	1500	30	60	1.39	1.39	2.95	1.54	129.6
9	1750	30	60	7.86	7.86	1.78	1.84	128.6
10	2250	30	60	5.30	5.30	1.55	1.81	123.5
11	2500	30	60	4.22	4.22	1.39	1.86	124.1
12	3000	30	60	3.87	3.87	1.15	1.55	123.9
13	2000	5	60	1.07	6.42	1.23	2.50	124.7
14	2000	15	60	3.58	7.16	1.36	1.70	122.4
15	2000	45	60	10.88	7.25	3.85	2.07	127.6
16	2000	60	60	11.29	5.65	5.59	2.19	127.6
17[e]	2000	30	60	1.12	1.12	1.36	1.67	122.5
18[f]	2000	30	60	0.01	0.01	—	—	—

[a] Conditions: 2.0 μmol of **Fe5**, 100 mL of toluene, 10 atm C$_2$H$_4$. [b] Values in units of 10^6 g (PE) per mol (Fe) per h. [c] M_w in units of kg mol^{-1}. M_w and M_w/M_n determined by GPC. [d] Determined by DSC. [e] 5 atm C$_2$H$_4$. [f] 1 atm C$_2$H$_4$.

Table 4 Ethylene polymerization results obtained using **Fe1–Fe8** using either MMAO or MAO as activator[a]

Entry	Precat.	Activator	Al : Fe	T (°C)	PE mass (g)	Activity[b]	M_w[c]	M_w/M_n[c]	T_m[d]
1	**Fe1**	MMAO	2000	60	24.55	24.55	42.32	11.85	128.2
2	**Fe2**	MMAO	2000	60	25.20	25.20	62.41	18.27	129.0
3	**Fe3**	MMAO	2000	60	13.46	13.46	7.73	2.67	128.6
4	**Fe4**	MMAO	2000	60	5.29	5.29	1.36	1.61	121.6
5	**Fe5**	MMAO	2000	60	9.38	9.38	1.47	1.97	125.0
6	**Fe6**	MMAO	2000	60	1.51	1.51	2.59	2.26	126.5
7	**Fe7**	MMAO	2000	60	21.35	21.35	9.38	7.06	126.5
8	**Fe8**	MMAO	2000	60	13.56	13.56	25.51	7.38	130.3
9	**Fe1**	MAO	2500	40	6.71	6.71	36.81	23.87	129.1
10	**Fe2**	MAO	2500	40	5.16	5.16	210.56	80.40	134.7
11	**Fe3**	MAO	2500	40	3.55	3.55	167.46	24.20	133.7
12	**Fe4**	MAO	2500	40	3.46	3.46	176.56	17.00	135.1
13	**Fe5**	MAO	2500	40	6.01	6.01	94.07	12.14	134.3
14	**Fe6**	MAO	2500	40	1.22	1.22	185.46	16.94	136.0
15	**Fe7**	MAO	2500	40	7.22	7.22	13.07	5.97	128.7
16	**Fe8**	MAO	2500	40	6.17	6.17	130.26	71.18	133.4
17	**Fe2**	MMAO	2000	80	7.74	7.74	1.80	1.54	124.5
18	**Fe2**	MMAO	2000	100	0.63	0.63	0.68	1.87	130.5
19	**Fe7**	MAO	2500	80	8.54	8.54	8.63	6.76	126.4
20	**Fe7**	MAO	2500	100	3.92	3.92	7.06	6.84	126.6

[a] Conditions: 2.0 µmol of iron precatalyst, 100 mL of toluene, 10 atm C_2H_4, 30 min. [b] Values in units of 10^6 g (PE) per mol (Fe) per h. [c] M_w in units of kg mol^{-1}. M_w and M_w/M_n determined by GPC. [d] Determined by DSC.

Ethylene polymerization using Fe5/MMAO. With **Fe5**/MMAO employed as the initial catalyst system to be studied, the impact of temperature on the polymerization runs was firstly explored by running the reactions between 30 and 80 °C with the Al : Fe molar ratio fixed at 2000, the run time at 30 min and ethylene pressure at 10 atm (entries 1–6, Table 2).

Inspection of the results showed that **Fe5**/MMAO reached its highest activity of 9.38×10^6 g (PE) per mol (Fe) per h at 60 °C (entry 4, Table 2), while further increasing the temperature to 80 °C, saw a rapid decrease in activity reaching a minimum of 0.57×10^6 g (PE) per mol (Fe) per h. This obvious drop-off in performance at >60 °C can be ascribed to a combination of factors including the lower solubility of ethylene[14] and the partial deactivation of the active species.[15] These variations in temperature were also found to impact on the molecular weight of the polyethylene, with a sharp decrease from 11.92 to 2.30 kg mol^{-1} noted on increasing the temperature from 30 °C to 40 °C, then as the temperature was raised beyond 40 °C a more gradual

decrease was observed reaching a value of 0.55 kg mol^{-1} at 80 °C (Fig. 3). This decrease in M_w can be ascribed to the greater rate of chain termination that occurs at higher run temperatures.[16] In addition, all these low molecular weight polymers exhibited narrow and unimodal dispersities (M_w/M_n range: 1.5–2.2), as well as relatively low melting temperatures (T_m range: 122–127 °C), findings that show some differences when compared with the majority of polymers generated using related iron catalysts.[5f,7,8,10,11] Significantly, these characteristics lend themselves to potential industrial applications that require low molecular weight polyethylene waxes.[5,17]

Subsequently, the amount of MMAO was examined by varying the Al : Fe molar ratio of MMAO from 1500 to 3000 with the temperature kept at 60 °C (entries 4, 8–12, Table 2). Examination of the results employing **Fe5**/MMAO reveals a peak activity of 9.38×10^6 g (PE) per mol (Fe) per h at a ratio of 2000 (entry 4, Table 2). On the other hand, the highest molecular weight polymer of 2.95 kg mol^{-1} was achieved with the lowest amount of MMAO (Al : Fe = 1500) and then gradually declined to 1.15 kg mol^{-1} as the Al : Fe molar ratio increased. This downward trend can likely be attributed to the onset of chain transfer from the active iron species to the aluminum activator resulting in shorter chain polymers.[8,10d] Meanwhile, the dispersities of the polymers remained narrow (M_w/M_n range: 1.5–2.0), differing notably from those obtained using **A–C** (Chart 1) which exhibited, in most cases, higher molecular weights and broader distributions with some bimodal character.[3,9a,10a,11a]

Thirdly, the performance of **Fe5**/MMAO over time was studied by conducting polymerization runs at selected time intervals between 5 and 60 min with the temperature and Al : Fe molar ratio kept at 60 °C and 2000 : 1, respectively (entries 4, 13–
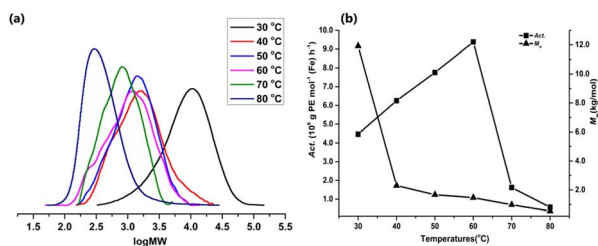
Fig. 3 For **Fe5**/MMAO: (a) GPC traces displaying log M_W of the polymer as a function of reaction temperature (entries 1–6, Table 2) and (b) plots of catalytic activity and M_w of the polymer *versus* reaction temperature.
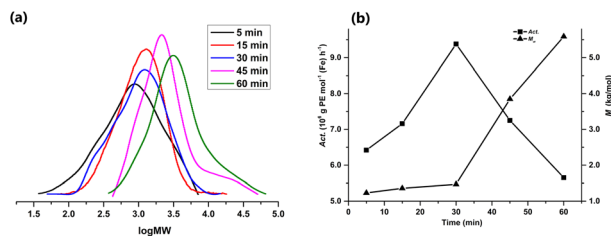
Fig. 4 For **Fe5**/MMAO: (a) GPC traces displaying log M_W of the polymer as a function of reaction time (entries 4, 13–16, Table 2) and (b) plots of catalytic activity and M_w of the polymer *versus* reaction time.

Fig. 5 For **Fe5**/MAO: (a) GPC traces displaying log M_W of the polymer as a function of reaction temperature (entries 1–5, Table 3) and (b) plots of catalytic activity and M_w of the polymer *versus* reaction temperature.

Fig. 6 For **Fe5**/MAO and **Fe5**/MAO, comparison of (a) activity *versus* reaction temperature and (b) polyethylene molecular weight *versus* reaction temperature.

16, Table 4). The upper most activity of 9.38×10^6 g (PE) per mol (Fe) per h was found after 30 min which suggests an appreciable induction time to fully generate the active species.[18] Further prolonging the reaction time to 60 min, saw only *ca.* 40% loss of activity, underlining the stability and slow deactivation of this catalyst over more extended run times.[19,20] In addition, the molecular weight of the PE wax showed some notable variation 1.23–5.59 kg mol^{-1} that is further borne out in the GPC traces (Fig. 4). Evidently, sufficient potency of the catalyst was retained despite the steady deactivation, highlighting the propensity of the active species to sustain chain growth.[11,20]

Fourthly, further polymerization runs were undertaken to explore the effect of ethylene pressure on the performance of **Fe5**/MMAO. Notably, as the pressure was lowered from 10 atm to 1 atm, a sharp drop-in activity from 9.38 to 0.01×10^6 g (PE) per mol (Fe) per h (*ca.* one thousand times loss) was observed (entries 4, 16, 17, Table 2). A less dramatic drop in performance was seen when the run was performed at 5 atm (entry 16 *vs.* entry 4, Table 2), with the molecular weight of the polymer remaining almost unchanged. It would appear that the propagation steps of coordination and insertion are less effective below a critical ethylene pressure for this catalyst system.[21] Additionally, the lower solubility of the ethylene monomer in reaction solvent at lower ethylene pressures may also be a possible contributing factor.[14a]

Ethylene polymerization using Fe5/MAO. To allow a comparison with the **Fe5**/MMAO runs and also to allow the identification of an effective set of reaction conditions, the performance of **Fe5**/MAO was subject to a similar set of optimization runs; the results of the evaluation are tabulated in Table 3. In terms of the run temperature, 40 °C was recognized as optimal whereby the highest activity of 4.99×10^6 g (PE) per mol (Fe) per h was observed (entry 2, Table 3). On raising the run temperature to 70 °C, the activity decreased sharply to 0.41×10^6 g (PE) per mol (Fe) per h (entry 5, Table 2). In terms of the response of the polymer M_w to temperature when using **Fe5**/MMAO, this was found to decrease steadily from 120.97 to 80.49 kg mol^{-1} as the temperature was increased from 30 °C to 70 °C (entries 1–5, Table 2, see Fig. 5), in line with the higher rate of chain termination.[22]

In comparison with **Fe5**/MMAO, not only was the optimal run temperature lower for **Fe5**/MAO, but also the general catalytic activity was reduced across the temperature range examined (see Fig. 6a). Additionally, the molecular weight of the
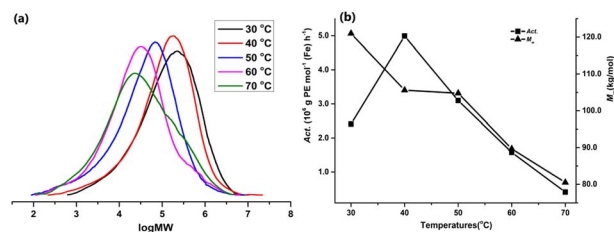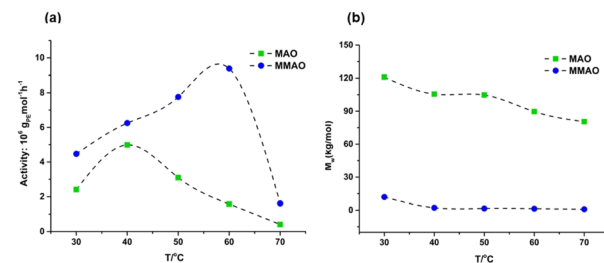
polyethylene obtained using MAO was nearly one hundred times that seen with MMAO (Fig. 6b), and what is more displayed broader distributions (M_w/M_n = 14.0–17.1) and higher T_m values (range: 135.9 to 134.2 °C). It is uncertain as to the reason behind this molecular weight difference but plausibly derives from the greater stability of the active species toward propagation over chain transfer.[8c] Alternatively, the higher amounts of trialkylaluminum species that are present in commercial samples of MMAO as compared to that in MAO, likely increases the rate of chain transfer and in turn a reduction in molecular weight.[8,23] It is also worth re-emphasizing that the aforementioned **Fe5**/MMAO system afforded polymers of narrower distribution and over a wider temperature range (M_w/M_n range: 2.2–1.5 between 30–80 °C), which would suggest that the polymerizations promoted by MAO are in general less controlled than that with MMAO.[24]

In regard to the most favorable Al : Fe ratio, 2500 was found to be optimum with the activity achieving its highest value of 6.01×10^6 g (PE) per mol (Fe) per h with the run temperature fixed at 40 °C (entry 8, Table 3). On the other hand, as the ratio was increased from 1500 to 3500, the molecular weight of the polymer reached its highest value of 105.58 kg mol^{-1} at 2000 then gradually declined reaching a minimum of 36.37 kg mol^{-1} at 3500 (entries 2, 6–10, Table 3). It would appear that above a critical amount of activator more facile chain transfer from iron to aluminum takes place.[25] Once again, the polymers obtained using **Fe5**/MAO displayed broad dispersities over the range in molar ratios (M_w/M_n range: 11.1–15.0).

As was observed with **Fe5**/MMAO, **Fe5**/MAO took 30 min to attain peak activity in this case reaching a value of 6.01×10^6 g

(PE) per mol (Fe) per h. Evidently, the induction period remains similar irrespective of the activator employed (entries 8, 11–14, Table 3). However, for run times in excess of 30 min, slow deactivation was observed with the activity reaching a minimum value of 3.61×10^6 g (PE) per mol (Fe) per h after 1 h. With respect to the polymer molecular weight, this was found to progressively increase (from 1.5 to 133.1 kg mol^{-1}) over time with gradual broadening in the distributions evident (M_w/M_n: from 13.5 to 22.2) (Fig. S1). Of note, the dramatic increase in molecular weight seen between 5 min and 15 min may be related to the rapid formation of the active species after 5 min.[7,8,20] On lowering the ethylene pressure to 5 atm (entry 15, Table 3), a decline in activity (0.92×10^6 g (PE) per mol (Fe) per h) was observed. Further lowering the pressure to 1 atm, led to only a trace amount of polymer being obtained.[21]

Evaluation of Fe1–Fe8 using MAO or MMAO. In order to understand how the variations in the N-aryl group substitution pattern affect performance and polymer properties, the remaining seven precatalysts, **Fe1–Fe4** and **Fe6–Fe8**, were screened employing the optimized polymerization conditions established independently for **Fe5**/MMAO (viz., Al : Fe = 2000, T = 60 °C) and **Fe5**/MAO (viz., Al : Fe = 2500, T = 40 °C). The full set of data alongside that for **Fe5** are presented in Table 4.
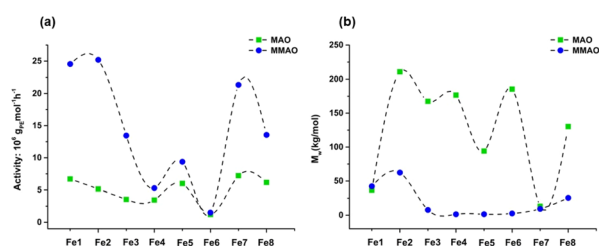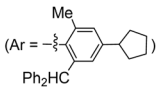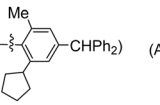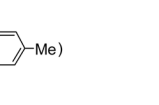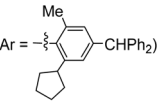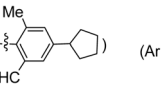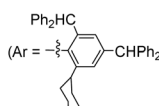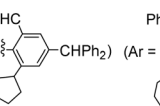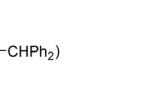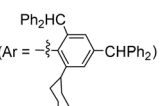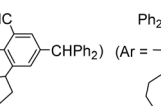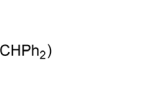
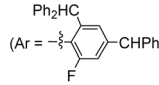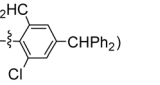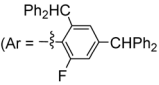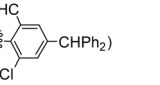

Fig. 7 Plots of (a) catalytic activity and (b) polyethylene molecular weight as a function of iron precatalyst for both MAO or MMAO activation.

In general, the MMAO-promoted polymerizations showed superior catalytic activity [activity range: 1.51–25.20×10^6 PE per (mol of Fe) per h. M_w: 1.36–62.41 kg mol^{-1}] but lower molecular weights for their polymers than their MAO-promoted counterparts [activity range: 1.22–6.71×10^6 g PE per (mol of Fe) per h; M_w: 13.07–210.56 kg mol^{-1}, Fig. 7]. Moreover, the MAO runs were less controlled with dispersities that were generally broader [M_w/M_n range: 6.0–80.4 (MAO) vs. 1.5–18.3 (MMAO)].

The relative order of catalytic activity for the three sub-classes of iron precatalyst, **E–G** (Chart 1) is shown in Table 5 for each activator. From inspection of the table, it evident that the orders are essentially the same regardless of the activator employed.[18b,26] However, several other points emerge with regard to each sub-class of iron precatalyst. Firstly, for the **E**-class (**Fe1–Fe3**), the type of substituent positioned at the ortho-position of the N-aryl group greatly impacted the catalytic activity with **Fe1** and **Fe2**, containing the least steric hindrance being the most active. Evidently, the increased steric hindrance to ethylene coordination and insertion leads to lower polymerization rates.[8c,10b,12] Secondly, similar trends were also observed for **F** (**Fe4–Fe6**) in which the presence of most sterically bulky ortho-combination of benzhydryl and cyclooctyl results in the least active system. Conversely, the combination of cyclohexyl and benzhydryl at the ortho-position outperforms the less bulky cyclopentyl/benzhydryl ortho-pairing indicating the optimum steric hindrance is seen with the former, whereby the flexibility of the ortho-cyclohexyl ring likely exerts the most suitable protection to the metal center in the active catalyst but does not prevent the approach of the ethylene monomer; related observations have been noted elsewhere.[8b,27] Thirdly, **Fe7** containing the strongly electron-withdrawing fluoride showed much higher activity than its ortho-chloride counterpart **Fe8**, highlighting the increased Lewis acidic character of the cationic active species will in turn have a positive impact on catalytic activity.[13]

While steric factors are clearly influential on catalytic activity, they also impact on the molecular weight of the

Table 5 Relative order of catalytic activity for the three sub-classes of iron precatalyst, E–G (Chart 1)

polymers by inhibiting chain transfer.[28] Indeed, the range in molecular weights of the polymers produced using **Fe1–Fe8** with either MAO or MMAO was much broader than seen with structurally related analogues. In particular, by having a bulky –CHPh$_2$ group at the *ortho*-position greatly increases the molecular weight with the result that **Fe2** afforded the polymer with the highest level for both MAO or MMAO (MMAO: 62.41 kg mol^{-1}; MAO: 210.56 kg mol^{-1}). It is also evident that the ring size of the cycloalkyl group also affected the molecular weight with the bulkiest cyclooctyl-containing **Fe6** affording higher molecular weight than for **Fe4** and **Fe5**.[8b,c] The nature of the *para*-substituent also appears to be influential on the molecular weight of the polymer. For example, when comparing the polymer obtained by *para*-CHPh$_2$ **Fe4**/MMAO with *para*-methyl **Fe3**/MMAO, it is evident that the *para*-CHPh$_2$ group has a negative effect on molecular weight indicating the latter *para*-methyl systems allow more efficient propagation. Curiously, for the MAO-promoted system the opposite trend is noted with the molecular weight of the polymer formed by **Fe4**/MAO obviously higher than **Fe3**/MAO. This explanation behind these observations is unclear but plausibly derives from the differing activation processes that occur for MMAO over MAO. As a final point, the large variations in molecular weights seen using *ortho*-chloride **Fe8** (MMAO: 25.51 kg mol^{-1}. MAO: 130.26 kg mol^{-1}) and *ortho*-fluoride **Fe7** (MMAO: 9.38 kg mol^{-1} MAO: 13.07 kg mol^{-1}), further highlight the influence of the electron-withdrawing group at the *ortho*-position.[10b,13]

To examine the response of the most active iron systems identified from the independent MMAO and MAO studies to higher operating temperatures, we selected **Fe2**/MMAO [activity = 25.2×10^6 PE per (mol of Fe) per h at 60 °C] and **Fe7**/MAO [activity = 7.22×10^6 PE per (mol of Fe) per h at 40 °C], for further evaluation. Specifically, polymerization runs for each were conducted at 80 °C and 100 °C (entries 17–20, Table 4). Both of these catalyst systems exhibited excellent thermal stability when compared with previously reported analogues.[7–11]

Nonetheless, on the basis of the level of activity, it could be seen that the thermal stability of **Fe7**/MAO [3.92×10^6 PE per (mol of Fe) per h at 100 °C] is significantly higher than that for **Fe2**/MMAO [0.63×10^6 PE per (mol of Fe) per h at 100 °C, Table 2] and also when compared to the related iron system, **Fe5**/MAO [0.41×10^6 PE per (mol of Fe) per h at 70 °C, Table 2]. These observations highlight the positive effect of electron-withdrawing fluoride group on protecting the active center at higher temperature; similar phenomenon have been noted elsewhere.[10b,13] Additionally, it is evident that the ligand structure has a significant effect on the optimal run temperature with **Fe7**/MAO operating markedly better at 80 °C than the optimum of 40 °C identified when using **Fe5**/MAO.

Comparison of Fe1 and Fe4 with structurally related literature reports. In order to broaden the comparison of structural effects of the iron precatalyst beyond those described in this work, we have extracted data from previous work based on singly fused **D** (Chart 1) precatalysts bearing similar benzhydryl/cyclopentyl *ortho*-pairings (*viz.*, **Fe7a**,[8b] and **Fe7b**,[8c] Chart 2) as those in **Fe1** and **Fe4**. In addition, data for the 2,6-di-isopropylphenyl member of the 2-imino-6,7-dihydroquinlin-8(5H)-imine-ferrous chloride family of complexes, **Fe2,6-diPr**,[7] is presented for comparison; all polymerization runs were performed with MMAO as activator at $P_{C_2H_4} = 10$ atm with their optimal run temperature.

Inspection of Chart 2 reveals several points. Firstly, the catalytic activity follows the trends **Fe7a–Fe7b** and **Fe1 > Fe4** indicating that the presence of a benzhydryl group on the *ortho*-substituent leads to lower activity, as well as a decrease in the molecular weight of the polymer. This finding can be attributed to the excessive protection of the active iron center imparted by the bulky group that in turn impedes ethylene coordination and insertion.[28] Secondly, the introduction of cyclopentyl group on the *ortho*-position shows a positive effect on catalytic activity, as evidenced by **Fe1** being much more active and thermally stable than **Fe2,6-diPr**, which is likley due to the unique steric effect

	Fe7a[8b]	**Fe7b**[8c]	**Fe2,6-diPr**
Activity [g PE mol^{-1} h^{-1}]	16.1×10^6	15.3×10^6	12.6×10^6
M_w (kg mol^{-1})	7.4	27.2	29.9
M_w/M_n	4.3	4.2	8.9

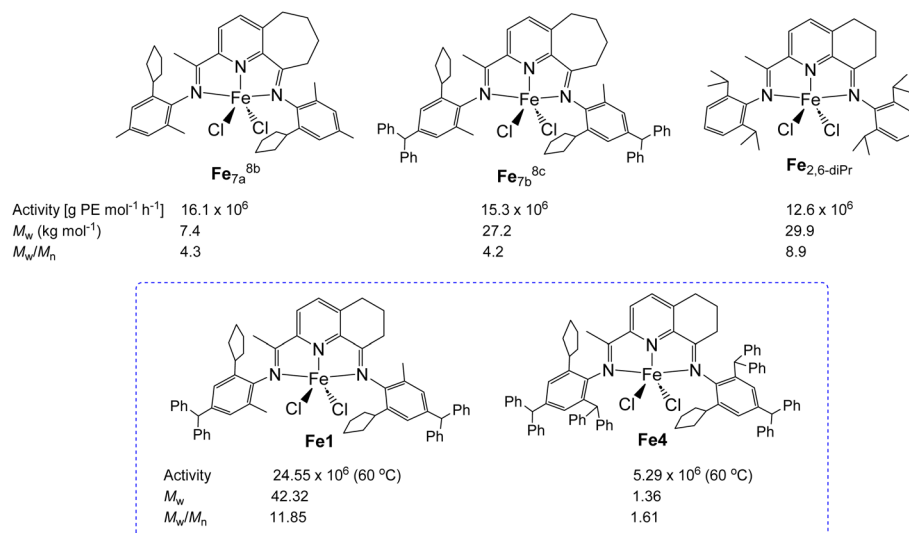|	**Fe1**	**Fe4**
Activity	24.55×10^6 (60 °C)	5.29×10^6 (60 °C)
M_w	42.32	1.36
M_w/M_n	11.85	1.61

Chart 2 Comparison of catalytic activity and polymer properties displayed using **Fe1** and **Fe4** with structurally related **Fe7a**[8b] **Fe7b**[8c] and **Fe2,6-diPr**;[7] in each case activation with MMAO at $P_{C_2H_4} = 10$ atm.

© 2025 The Author(s). Published by the Royal Society of Chemistry

imparted by the cycloalkyl ring.[8b,10c,18a] Thirdly, this comparison further highlights the low molecular weight polyethylene waxes that are obtained using **Fe4**/MMAO, that display much narrower dispersities than that seen in previous reports.[8,10] We consider the formation of such materials is driven by the combined effect of the *N*-aryl cycloalkyl and benzhydryl groups on the polymerization process.[12,24]

Microstructural analysis of polyethylene

As can be gathered from Tables 2–4, all polyethylenes prepared in this work display melt temperatures that exceed 121 °C which suggests high linearity (Tables 2–4). To provide some supporting evidence for this, as well as explore any correlations that exist between reaction conditions or precatalyst structure and structural properties of the polymers, four representative polymer samples prepared using (i) **Fe7**/MAO at 40 °C (M_w = 13.07 kg mol^{-1}, entry 15, Table 4), (ii) **Fe7**/MAO at 100 °C (M_w = 7.06 kg mol^{-1}, entry 20, Table 4), (iii) **Fe5**/MMAO at 60 °C (M_w = 1.47 kg mol^{-1}, entry 5, Table 4) and (iv) **Fe4**/MMAO at 60 °C (M_w = 1.36 kg mol^{-1}, entry 4, Table 4) were studied using high-temperature ^{1}H and ^{13}C NMR spectroscopy (Fig. 8 and 9 and S2–S7).[29]

In general, the ^{1}H NMR spectra for all samples displayed as the most downfield signals two low intensity multiplets at around δ 5.89 (H$_b$) and δ 5.03 (H$_a$), integrating to 1 and 2, respectively, that are assignable to a vinyl end group (–CH=CH$_2$). Evidently, it can be inferred that β-H elimination pathway is operational during the termination pathway of the polymerization process for all of these iron catalysts.[1b,5f,30] More upfield can be seen a multiplet at around δ 2.11 ppm for the protons (H$_c$) adjacent to the vinyl end group while a high intensity

Fig. 9 1D sequence inverse-gated decoupled ^{13}C NMR spectrum of the polyethylene obtained using **Fe4**/MMAO at 60 °C (entry 4, Table 4); recorded in tetrachloroethane-*d*$_2$ at 100 °C.

singlet peak at 1.36 ppm corresponds to the –(CH$_2$)– repeat unit. As the most upfield peak at *ca.* δ 0.96 ppm, can be found the chain-end methyl group (H$_g$). For all 4 polymer samples, the ratio of the chain-end methyl (H$_g$) to the vinyl protons (H$_a$/H$_b$) exceeds 3 : 3 that would be expected for a perfectly linear vinyl-terminated polyethylene. This finding implies the polymers are additionally composed of some fully saturated polymer that can be credited to the coexistence of a termination pathway based on chain transfer to aluminium.[5f,11,31] A mechanistic pathway to account for the different types of polymer end-group generated by these iron catalysts is shown in Fig. S8. Interestingly for the two samples produced using **Fe7**/MAO, the ratio of the chain-end methyl to the vinyl protons shows some variation with run temperature. In particular, the polymer obtained at 100 °C possessed a higher content of vinyl end groups than at 40 °C, with the ratio of chain-end methyl protons (H$_g$) to the H$_a$ vinyl protons decreased from 9.2 : 2.0 to 6.8 : 2.2 (Fig. 8a and S2). This observation suggests a higher level of vinyl-terminated polymer at higher run temperature in line with β-H elimination termination becoming more prevalent as a termination pathway (Fig. S8).[3e,6b]

Confirmation of the vinylic functionality in all polymer samples is provided in the ^{13}C NMR spectra with vinylic carbons at around δ 114.4 (C$_a$) and 139.6 (C$_b$), while the carbon signal for the –(CH$_2$)– repeat unit is seen as a high intensity singlet at δ 30.00 ppm. Other less intense upfield peaks in the ^{13}C NMR spectrum can be seen that vary dependent on the particular polymer. For that generated using **Fe7**/MAO at either run temperature (M_w = 7.06 kg mol^{-1}, entry 20, Table 4) (Fig. 8b and S3), the polymers displayed signals at around δ 32.2 (C$_e$), 22.9 (C$_f$) and 14.3 (C$_g$) can be attributed to a saturated propyl end-group. On the other hand, for that produced using **Fe5**/MMAO signals for *n*-propyl groups were also found in their ^{13}C NMR spectrum, but were supplemented by additional weak peaks at around δ 22.9, 27.7, 28.3 and 39.5 which can be ascribed to an isobutyl end group (Fig. S4 and S5). Such an observation would suggest that the chain transfer to aluminium mentioned above
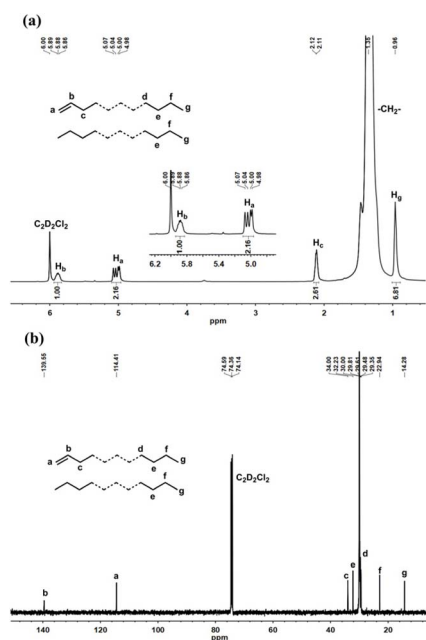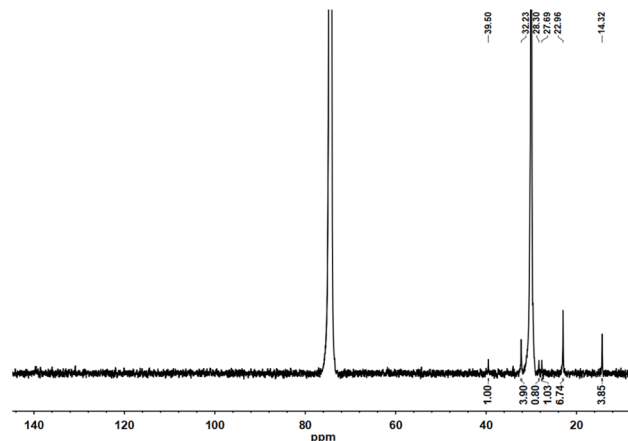

Fig. 8 For the polyethylene obtained using **Fe7**/MAO at 100 °C, (a) the ^{1}H NMR spectrum, including an expansion of the vinylic region, and (b) ^{13}C NMR spectrum (entry 21, Table 4); both recorded in tetrachloroethane-*d*$_2$ at 100 °C.

is responsible in this case making use of Al(i-Bu)$_3$ present within the MMAO.[3d,5f,10d]

To explore the effect of cycloalkyl ring size on the polymer microstructure, the ^{1}H NMR spectrum for the PE samples prepared using cyclopentyl-containing **Fe4**/MMAO (Fig. S4 and S5) were compared with that obtained for cyclohexyl **Fe5**/MMAO (Fig. S6 and S7); both samples were generated at a run temperature of 60 °C. Scrutiny of their ^{1}H NMR spectra revealed distinct variations in the relative amounts of fully saturated (based on n-propyl and isobutyl) and vinyl chain-ends, with the ratio of the integrals for H$_g$ to H$_a$ protons for **Fe5**/MMAO being noticeably less (H$_g$: H$_a$ ratio = 42.4 : 1.95 **Fe4**/MMAO vs. 25.8 : 2.07 in **Fe5**/MMAO). This finding would suggest that the relative amounts of these distinct type of polymer chain end can also be regulated by adjusting the steric hindrance of the ligands with chain transfer to aluminum becoming the dominant pathway for **Fe4**/MMAO (Fig. S8). Furthermore, this finding is consistent with the molecular weight generated from **Fe4**/MMAO being less than that in **Fe5**/MMAO. To further underscore the importance of chain transfer to aluminum using **Fe4**/MMAO, the inverse-gated decoupled ^{13}C NMR spectrum was also recorded (Fig. 9), revealing an integral ratio for C$_g$ and C$_c$ of 3.9 : 1.0, while the vinylic C$_{a/b}$ was almost unobservable in line with its extremely low content.[32,33]

Conclusions

In summary, eight examples of 2-imino-6,7-dihydroquinlin-8(5H)-imine-iron complexes, **Fe1–Fe8**, that can be divided into 3 sub-classes (**E**, **F** and **G**, Chart 1) depending on the N-aryl substitution pattern, have successfully prepared by a one-pot route. Full characterization of these iron(II) complexes has been undertaken including in two cases by single-crystal X-ray diffraction. In the presence of MAO or MMAO, all eight complexes showed high catalytic activities for ethylene polymerization with N-2-Me-4-(C$_5$H$_9$)-6-(CHPh$_2$)C$_6$H$_2$-containing **Fe2**/MMAO the highest at 25.20 × 10^6 g (PE) per mol (Fe) per h, which proved superior to its previously reported fused-ring counterparts **C** and **D** (Chart 1). This highlights the beneficial effect of combining benzhydryl and cycloalkyl group at specific substitutions on chain propagation. Subsequent investigation of the electronic effect of benzhydryl substitution at the para-position of the N-aryl group showed opposing effects on the catalytic performance that were dictated by the nature of the activator. Notably, the 2-cycloalkyl-4,6-benzhydryl substituted class, **Fe4–Fe6** (**F**, Chart 1), under MMAO-activation generated wax-like polymer with the lowest molecular weight and narrowest dispersity (M_w/M_n range: 1.6–2.3); characteristics that are quite distinct from their most closely related iron comparators. Indeed, such a molecular weight range for the polyethylene (M_w: 1.36–2.59 kg mol^{-1}) falls in the range used in commercial polyethylene waxes. End-group analysis of the polymers formed using **Fe7**/MAO, **Fe5**/MMAO and **Fe4**/MMAO provided evidence for both β-hydrogen elimination and chain transfer to aluminum being operative during chain termination, with run temperature, ligand structure and the type of activator being influential on this termination event. In short, this work highlights how the catalytic performance and polymer characteristics can be regulated by targeted variations in the ligand structures (via electronic and steric properties) and polymerization conditions (especially the nature of the activator).

Experimental

General considerations

All air- and moisture-sensitive compounds were manipulated under an atmosphere of nitrogen by employing standard Schlenk techniques. Toluene was heated to reflux over sodium for 12 h under nitrogen and then distilled immediately before use in the polymerization runs. The ^{13}C and ^{1}H NMR spectra of the polyethylene were all recorded on a Bruker AVANCE III 500 MHz instrument in 5 mm standard glass tubes at 100 °C using 1,1,2,2-tetrachloroethane-d_2 (C$_2$D$_2$Cl$_4$) as solvent with TMS as an internal standard. Sample preparation involved the dissolution of pre-weighed amount of polyethylene (20–40 mg) in 1,1,2,2-tetrachloroethane-d_2 (1 mL) at elevated temperature before transferring a portion of this to the NMR tube for analysis. The molecular weight (M_w) and dispersity (M_w/M_n) of the polyethylene were determined by operating a PL-GP220 instrument at 150 °C using 1,2,4-trichlorobenzene as the eluting solvent. The true average molecular weights of the polyethylenes were achieved by inputting the Mark–Houwink constants of polyethylene; K (0.727) and α (40.6) were provided by PL Company (Beijing, China). The samples were dissolved at a concentration of 1.0 to 2.5 mg mL^{-1}, depending on the molecular weights. The melting temperatures of the polyethylene (T_m) was measured from the second scanning run on a PerkinElmer TA-Q2000 differential scanning calorimetry (DSC) analyzer under a nitrogen atmosphere. Sample preparation involved heating a 5.0 mg sample of polyethylene to 160 °C at a rate of 20 °C per min and then maintaining this at 160 °C for 3 min to remove any thermal history; the sample was subsequently cooled to −40 °C at a rate of 20 °C per min. Infrared (IR) spectra were recorded on a PerkinElmer System 2000 FT-IR (Fourier Transform Infrared) spectrometer while elemental analysis was performed using a Flash EA 1112 microanalyzer. The aluminum-alkyls, MAO (MAO, 1.46 M in toluene) and MMAO (MMAO, 1.93 M in heptane) were purchased from Akzo Nobel Corp. High-purity ethylene was purchased from Beijing Yansan Petrochemical Company. The compound, 2-acetyl-6,7-dihydroquinolin-8(5H)-one,[7] and the anilines namely, 2-methyl-4-benzhydryl-6-cyclopentylaniline, 2-methyl-4-cyclopentyl-6-benzhydrylaniline, 2-cyclopentyl-4-methyl-6-benzhydrylaniline, 2-cyclopentyl-4,6-dibenzhydrylaniline, 2-cyclohexyl-4,6-dibenzhydrylaniline, 2-cyclooctyl-4,6-dibenzhydrylaniline, 2-fluoro-4,6-dibenzhydrylaniline and 2-chloro-4,6-dibenzhydrylaniline were prepared as previously described.[34] All other reagents were purchased from Aldrich, Acros or local suppliers.

Synthesis of [2-(ArN=CCH$_3$)-8-(ArN)C$_9$H$_8$N]FeCl$_2$ (Fe1–Fe8)

Ar = 2-Me-4-(CHPh$_2$)-6-(C$_5$H$_9$)C$_6$H$_2$ Fe1. Under a nitrogen atmosphere, a mixture of 2-acetyl-6,7-dihydroquinolin-8(5H)-

one (0.05 g, 0.25 mmol), 2-methyl-4-benzhydryl-6-cyclopentylaniline (0.19 g, 0.55 mmol) and $FeCl_2 \cdot 4H_2O$ (0.05 g, 0.25 mmol) in glacial acetic acid (5 mL) was stirred and heated to reflux for 3 h. Once cooled to room temperature, freshly distilled diethyl ether (15 mL) was added to precipitate a solid which was filtered and collected. This solid was then re-dissolved in freshly distilled CH_2Cl_2 (1 mL) and diethyl ether added to induce precipitation and the resulting solid collected by filtration and dried under reduced pressure to give **Fe1** as a blue powder (0.18 g, 75%). FT-IR (KBr cm^{-1}): 2949 (w), 2863 (w), 1625 (w), 1595 (w), 1489 (w), 1448 (w), 1366 (w), 1265 (w), 1241 (w), 1201 (w), 1139 (w), 1030 (w), 929 (w), 896 (w), 743 (w), 702 (s). Anal. calc. for $C_{61}H_{61}Cl_2FeN_3$ (962.9): C, 76.09; H, 6.39; N, 4.36. Found: C, 76.13; H, 5.93; N, 4.11%.

Ar = 2-Me-4-(C_5H_9)-6-(CHPh$_2$)C$_6$H$_2$ Fe2. Using a similar procedure and molar ratios to that described for **Fe1** but with 2-methyl-4-cyclopentyl-6-benzhydrylaniline as the aniline, **Fe2** was isolated as a green powder (0.16 g, 67%). FT-IR (KBr cm^{-1}): 2948 (w), 2866 (w), 1620 (w), 1575 (w), 1490 (w), 1450 (w), 1374 (m), 1267 (w), 1243 (m), 1214 (w), 1154 (w), 1079 (w), 1033 (w), 924 (w), 869 (w), 825 (w), 749 (m), 703 (s). Anal. calc. for $C_{61}H_{61}Cl_2FeN_3$ (962.9): C, 76.09; H, 6.39; N, 4.36. Found: C, 75.72; H, 6.28; N, 4.20%.

Ar = 2-(C_5H_9)-4-Me-6-(CHPh$_2$)C$_6$H$_2$ Fe3. Using a similar procedure and molar ratios to that described for **Fe1** but with 2-cyclopentyl-4-methyl-6-benzhydrylaniline as the aniline, **Fe3** was isolated as a green powder (0.18 g, 75%). FT-IR (KBr cm^{-1}): 2951 (w), 2866 (w), 1603 (w), 1575 (w), 1493 (w), 1450 (w), 1373 (w), 1270 (w), 1243 (w), 1207 (w), 1137 (w), 1075 (w), 1033 (w), 933 (w), 863 (w), 924 (w), 748 (w), 701 (s). Anal. calc. for $C_{61}H_{61}Cl_2FeN_3$ (962.9): C, 76.09; H, 6.39; N, 4.36. Found: C, 75.88; H, 6.21; N, 4.29%.

Ar = 2-(C_5H_9)-4,6-(CHPh$_2$)$_2$C$_6$H$_2$ Fe4. Using a similar procedure and molar ratios to that described for **Fe1** but with 2-cyclopentyl-4,6-dibenzhydrylaniline as the aniline, **Fe4** was isolated as a green powder (0.17 g, 54%). FT-IR (KBr cm^{-1}): 2956 (w), 2868 (w), 1618 (w), 1599 (w), 1575 (w), 1494 (m), 1447 (w), 1366 (w), 1269 (w), 1241 (m), 1154 (w), 1075 (w), 1033 (w), 899 (w), 863 (w), 823 (w), 747 (m), 698 (s). Anal. calc. for $C_{85}H_{77}Cl_2FeN_3$ (1267.3): C, 80.56; H, 6.12; N, 3.32. Found: C, 80.08; H, 5.89; N, 3.36%.

Ar = 2-(C_6H_{11})-4,6-(CHPh$_2$)$_2$C$_6$H$_2$ Fe5. Using a similar procedure and molar ratios to that described for **Fe1** but with 2-cyclohexyl-4,6-dibenzhydrylaniline as the aniline, **Fe5** was isolated as a green powder (0.18 g, 56%). FT-IR (KBr cm^{-1}): 2925 (w), 2858 (w), 1624 (w), 1599 (w), 1569 (w), 1494 (w), 1447 (m), 1369 (w), 1272 (w), 1241 (w), 1075 (w), 1033 (w), 908 (w), 865 (w), 825 (w), 745 (m), 699 (s). Anal. calc. for $C_{87}H_{81}Cl_2FeN_3$ (1295.4): C, 80.67; H, 6.30; N, 3.24. Found: C, 80.22; H, 6.11; N, 3.19%.

Ar = 2-(C_8H_{15})-4,6-(CHPh$_2$)$_2$C$_6$H$_2$ Fe6. Using a similar procedure and molar ratios to that described for **Fe1** but with 2-cyclooctyl-4,6-dibenzhydrylaniline as the aniline, **Fe6** was isolated as a green powder (0.18 g, 53%). FT-IR (KBr cm^{-1}): 2918 (w), 2852 (w), 1605 (w), 1575 (w), 1494 (w), 1446 (w), 1367 (w), 1269 (w), 1241 (w), 1135 (w), 1077 (w), 1031 (w), 924 (w), 865 (w), 827 (w), 746 (w), 701 (s). Anal. calc. for $C_{91}H_{89}Cl_2FeN_3$ (1351.5): C, 80.87; H, 6.64; N, 3.11. Found: C, 80.39; H, 6.21; N, 3.14%.

Ar = 2-F-4,6-(CHPh$_2$)$_2$C$_6$H$_2$ Fe7. Using a similar procedure and molar ratios to that described for **Fe1** but with 2-fluoro-4,6-dibenzhydrylaniline as the aniline, **Fe7** was isolated as a green powder (0.20 g, 69%). FT-IR (KBr cm^{-1}): 2975 (w), 2909 (w), 1624 (w), 1602 (w), 1574 (w), 1494 (w), 1427 (w), 1297 (w), 1243 (w), 1125 (w), 1032 (w), 920 (w), 830 (w), 745 (w), 700 (s). Anal. Calc. for $C_{75}H_{59}Cl_2F_2FeN_3$ (1167.1): C, 77.19; H, 5.10; N, 3.60. Found: C, 76.87; H, 4.83; N, 3.50%.

Ar = 2-Cl-4,6-(CHPh$_2$)$_2$C$_6$H$_2$ Fe8. Using a similar procedure and molar ratios to that described for **Fe1** but with 2-chloro-4,6-dibenzhydrylaniline as the aniline, **Fe8** was isolated as a green powder (0.19 g, 63%). FT-IR (KBr cm^{-1}): 2970 (w), 2909 (w), 1605 (w), 1574 (w), 1491 (w), 1447 (w), 1406 (w), 1378 (w), 1241 (w), 1074 (w), 900 (w), 827 (w), 746 (w), 701 (s). Anal. calc. for $C_{75}H_{59}Cl_4FeN_3$ (1200.0): C, 75.07; H, 4.96; N, 3.50. Found: C, 74.63; H, 4.55; N, 3.52%.

X-ray crystallographic studies

Single crystals of **Fe3** and **Fe5** suitable for the X-ray determinations were obtained by layering heptane onto a dichloromethane solution of the corresponding complex at room temperature. With graphite monochromated Cu-Kα radiation (λ = 1.54184 Å) at 170(2) K, cell parameters were obtained by global refinement of the positions of all collected reflections. The data were corrected for Lorentz and polarization effects (SAINT) and semiempirical absorption corrections based on equivalent reflections were applied (SADABS). Using Olex2,[35] the structure was solved with the SHELXT[36a] structure solution program using Intrinsic Phasing and refined with the SHELXL[36b] refinement package using Least Squares minimisation. All hydrogen atoms were placed in calculated positions. Details of the X-ray structure determinations and refinements are provided in Table S1.

Procedures for ethylene polymerization

Ethylene polymerization at 5 or 10 atm C_2H_4. The polymerizations were undertaken in a stainless-steel autoclave (250 mL) with a built-in ethylene pressure control system, temperature controller and mechanical stirrer. In addition, the reactor is also equipped with a thermocouple to control the reaction temperature; any exotherm produced could be adjusted by adjusting the water flow in the steel tube inside the autoclave. The autoclave was first evacuated and backfilled with ethylene three times. When the required temperature was reached, the iron precatalyst (2.0 μmol), pre-dissolved in toluene (30 mL) in a Schlenk tube, was injected into the autoclave containing ethylene (*ca.* 1 atm) followed by the addition of more toluene (30 mL). The required amount of activator (MAO or MMAO) and additional toluene were added successively by syringe, taking the total volume of solvent to 100 mL. The autoclave was immediately pressurized with 5/10 atm of ethylene gas and the stirring initiated. After the required reaction time, the reactor was cooled with a water bath and the excess ethylene vented. Following quenching of the reaction with 10% hydrochloric acid in ethanol, the polymer was collected and washed with

ethanol. Once dried under reduced pressure at 50 °C, the polymer sample was weighed.

Ethylene polymerization at 1 atm C_2H_4. The polymerization at 1 atm C_2H_4 was carried out in a Schlenk tube. Under an ethylene atmosphere, **Fe5** (2.0 μmol) was added followed by toluene (30 mL) and then the required amount of activator (MAO, MMAO) introduced by syringe. The resulting solution was stirred at the required temperature under 1 atm of C_2H_4. After 30 min, the ethylene pressure was vented and the solution quenched with 10% hydrochloric acid in ethanol. The polymer was collected by filtration, dried under reduced pressure at 50 ° C until of constant weight.

Author contributions

Randi Zhang: data curation, investigation, writing – original draft. Yanping Ma: writing – editing, investigation, formal analysis. Gregory Solan: writing – review & editing. Yizhou Wang: data curation, investigation. Jiahao Gao: data curation, investigation. Tongling Liang: data curation, investigation. Wen-Hua Sun: writing – review & editing, concept and administration, and formal analysis.

Conflicts of interest

There are no conflicts to declare.

Data availability

The synthetic procedures for the iron complexes are presented in the text along with the analytical data. All raw data, such as NMR, GPC and DSC can be obtained upon request from the correspond author.

CCDC 2482813 (**Fe3**) and 2482814 (**Fe5**) contain the supplementary crystallographic data for this paper.[37a,b]

Supplementary information: the molecular structures and selected bond angles and bond lengths of **Fe3** and **Fe5** are presented in the text; and their CCDC number, crystal data and structure refinements. The detailed data in regard to the catalytic performances of all new iron complexes appear in the manuscript along with GPC curves and NMR spectra of representative polymers. More detailed GPC curves and NMR spectra. See DOI: https://doi.org/10.1039/d5ra06630a.

Notes and references

1 (a) G. J. P. Britovsek, V. C. Gibson, B. S. Kimberley, P. J. Maddox, S. J. McTavish, G. A. Solan, A. J. P. White and D. J. Williams, *Chem. Commun.*, 1998, 849–850; (b) G. J. P. Britovsek, M. Bruce, V. C. Gibson, B. S. Kimberley, P. J. Maddox, S. Mastroianni, S. J. McTavish, C. Redshaw, G. A. Solan, S. Stromberg, A. J. P. White and D. J. Williams, *J. Am. Chem. Soc.*, 1999, **121**, 8728–8740; (c) G. J. P. Britovsek, V. C. Gibson and D. F. Wass, *Angew. Chem., Int. Ed.*, 1999, **38**, 428–447.

2 (a) B. L. Small, M. Brookhart and A. M. A. Bennett, *J. Am. Chem. Soc.*, 1998, **120**, 4049–4050; (b) B. L. Small and M. Brookhart, *J. Am. Chem. Soc.*, 1998, **120**, 7143–7144.

3 (a) G. J. P. Britovsek, V. C. Gibson, B. S. Kimberley, S. Mastroianni, C. Redshaw, G. A. Solan, A. J. P. White and D. J. Williams, *J. Chem. Soc. Dalton Trans.*, 2001, 1639–1644; (b) T. M. Smit, A. K. Tomov, G. J. P. Britovsek, V. C. Gibson, A. J. P. White and D. J. Williams, *Catal. Sci. Technol.*, 2012, **2**, 643; (c) L. Guo, W. Zhang, F. Cao, Y. Jiang, R. Zhang, Y. Ma, G. A. Solan, Y. Sun and W.-H. Sun, *Polym. Chem.*, 2021, **12**, 4214–4225; (d) Q. Zhang, Z. Zuo, Y. Ma, T. Liang, X. Yang and W.-H. Sun, *Dalton Trans.*, 2022, **51**, 8290–8302; (e) K. F. Tahir, Y. Ma, Q. Mahmood, Y. Wang, G. Ren, S. Zou, H. Saeed, T. Liang and W.-H. Sun, *Polymer*, 2024, **308**, 127335; (f) S. Liu, Q. Li, Q. Mahmood, Z. Yu, Y. Wang, R. Zhang, G. Rend and W.-H. Sun, *React. Chem. Eng.*, 2025, **10**, 2030–2042; (g) Z. Hosseinzadeh, Q. Zhang, J. Gao, Y. Wang, Q. Wang, G. Ren, T. Liang, Y. Ma and W.-H. Sun, *Dalton Trans.*, 2025, **54**, 12590–12600; (h) Z. Hosseinzadeh, Q. Zhang, Q. Wang, A. M. Ashfaq, T. Liang, Y. Ma and W.-H. Sun, *ChemPlusChem*, 2025, **90**, e202500007; (i) M. Zada, Q. Zhang, Q. Mahmood, Y. Ma, Y. Sun and W.-H. Sun, *Dalton Trans.*, 2025, **54**, 7676.

4 (a) V. C. Gibson, C. Redshaw and G. A. Solan, *Chem. Rev.*, 2007, **107**, 1745–1776; (b) V. C. Gibson and G. A. Solan, *Metal Catalysts in Olefin Polymerization*, ed. Z. Guan, Springer, Berlin, Heidelberg, 2009, pp. 107–158; (c) V. C. Gibson and G. A. Solan, *Catalysis without Precious Metals*, ed. R. M. Bullock, Wiley-VCH, Weinheim, Germany, 2010, pp. 111–141.

5 (a) C. Bianchini, G. Giambastiani, L. Luconi and A. Meli, *Coord. Chem. Rev.*, 2010, **254**, 431–455; (b) W. Zhang, W.-H. Sun and C. Redshaw, *Dalton Trans.*, 2013, **42**, 8988–8997; (c) Z. Flisak and W.-H. Sun, *ACS Catal.*, 2015, **5**, 4713; (d) C. Bariashir, C. Huang, G. A. Solan and W.-H. Sun, *Coord. Chem. Rev.*, 2019, **385**, 208–229; (e) A. M. F. Phillips, H. Suo, M. d. F. C. G. da Silva, A. J. L. Pombeiro and W.-H. Sun, *Coord. Chem. Rev.*, 2020, **416**, 213332; (f) W. Zheng, Q. Mahmood, W. Zhang and W. H Sun, *Adv. Organomet. Chem.*, 2023, **79**, 41–83; (g) M. M. Meraz, W. Yang, W. Yang and W.-H. Sun, *J. Comput. Chem.*, 2023, **44**, 1–6; (h) M. Khoshsefat, Y. Ma and W.-H. Sun, *Materials*, 2025, **18**, 2123.

6 (a) Y. Wang, Z. Wang, Q. Zhang, Q. Wang, G. A. Solan, X. Duan, Y. Ma, J. Gao, Z. Zhou and W.-H. Sun, *Polym. Chem.*, 2025, **16**, 2718; (b) Y. Wang, Z. Wang, Q. Zhang, Y. Ma, G. A. Solan, Y. Sun and W.-H. Sun, *Catalysts*, 2024, **14**, 213.

7 W. Zhang, W. Chai, W.-H. Sun, X. Hu, C. Redshaw and X. Hao, *Organometallics*, 2012, **31**, 5039–5048.

8 (a) F. Huang, Q. Xing, T. Liang, B. Flisak, Z. Ye, X. Hu, W. Yang and W.-H. Sun, *Dalton Trans.*, 2014, **43**, 16818–16829; (b) J. Guo, W. Zhang, I. I. Oleynik, G. A. Solan,

I. V. Oleynik, T. Liang and W.-H. Sun, *Dalton Trans.*, 2020, **49**, 136; (*c*) M. Han, Q. Zhang, I. I. Oleynik, H. Suo, G. A. Solan, Y. Ma, I. V. Oleynik, T. Liang and W.-H. Sun, *Catalysts*, 2020, **10**, 1002.

9 (*a*) V. K. Appukuttan, Y. Liu, B. C. Son, C.-S. Ha, H. Suh and I. Kim, *Organometallics*, 2011, **30**, 2285; (*b*) W. Hou, C. Tang, G. Liu and Z. Huang, *Organometallics*, 2022, **41**, 3115–3121.

10 (*a*) S. Du, X. Wang, W. Zhang, Z. Flisak, Y. Sun and W.-H. Sun, *Polym. Chem.*, 2016, **7**, 4188–4197; (*b*) C. Bariashir, Z. Wang, Y. Ma, A. Vignesh, X. Hao and W.-H. Sun, *Organometallics*, 2019, **38**, 4455–4470; (*c*) H. Suo, Z. Li, I. V. Oleynik, Z. Wang, I. I. Oleynik, Y. Ma, Q. Liu and W.-H. Sun, *Appl. Organomet. Chem.*, 2020, **34**, e5937; (*d*) Q. Zhang, W. Yang, Z. Wang, G. A. Solan, T. Liang and W.-H. Sun, *Catal. Sci. Technol.*, 2021, **11**, 4605–4618; (*e*) W. Lin, L. Zhang, G. A. Solan and W.-H. Sun, *Eur. J. Inorg. Chem.*, 2021, **2021**, 4530–4538.

11 (*a*) Z. Wang, R. Zhang, W. Zhang, G. A. Solan, Q. Liu, T. Liang and W.-H. Sun, *Catal. Sci. Technol.*, 2019, **9**, 1933–1943; (*b*) Z. Wang, G. A. Solan, Y. Ma, Q. Liu, T. Liang and W.-H. Sun, *Research*, 2019, **2019**, e9426063.

12 R. Zhang, I. V. Oleynik, J. Li, G. A. Solan, Y. Ma, L. Jin, I. I. Oleynik, X. Hu and W.-H. Sun, *Eur. J. Inorg. Chem.*, 2021, **2021**, 3956–3968.

13 Q. Zhang, N. Wu, J. Xiang, G. A. Solan, H. Suo, Y. Ma, T. Liang and W.-H. Sun, *Dalton Trans.*, 2020, **49**, 9425–9437.

14 (*a*) D. P. Gates, S. A. Svejda, E. Oñate, C. M. Killian, L. K. Johnson, P. S. White and M. Brookhart, *Macromolecules*, 2000, **33**, 2320; (*b*) L. S. Lee, H. J. Ou and H. F. Hsu, *Fluid Phase Equilib.*, 2005, **231**, 221; (*c*) A. K. Tomov, V. C. Gibson, G. J. P. Britovsek, R. J. Long, M. van Meurs, D. J. Jones, K. P. Tellmann and J. J. Chirinos, *Organometallics*, 2009, **28**, 7033–7040.

15 (*a*) W.-H. Sun, X. B. Tang, T. L. Gao, B. Wu, W. J. Zhang and H. W. Ma, *Organometallics*, 2004, **23**, 5037–5047; (*b*) V. C. Gibson, C. Redshaw, G. A Solan, A. J. P. White and D. J. Williams, *Organometallics*, 2007, **26**, 5119–5123.

16 (*a*) R. Kempe, *Chem.–Eur. J.*, 2007, **13**, 2764; (*b*) H. Wang, W. Lu, H. Bi and S. Dai, *Polymer*, 2023, **273**, 125868.

17 G. J. P. Britovsek, S. A. Cohen, V. C. Gibson and M. van Meurs, *J. Am. Chem. Soc.*, 2004, **126**, 10701–10712.

18 (*a*) H. Suo, I. I. Oleynik, C. Bariashir, I. V. Oleynik, Z. Wang, G. A. Solan, Y. Ma, T. Liang and W.-H. Sun, *Polymer*, 2018, **149**, 45–54; (*b*) H. Suo, I. V. Oleynik, I. I. Oleynik, G. A. Solan, Y. Ma, T. Liang and W.-H. Sun, *Polymer*, 2021, **213**, 123294.

19 (*a*) D. J. Jones, V. C. Gibson, S. M. Green, P. J. Maddox, A. J. P. White and D. J. Williams, *J. Am. Chem. Soc.*, 2005, **127**, 11037–11046; (*b*) Z. Long, B. Wu, P. Yang, G. Li, Y. Liu and X.-J. Yang, *J. Organomet. Chem.*, 2009, **694**, 3793–3799.

20 T. Xiao, P. Hao, G. Kehr, X. Hao, G. Erker and W.-H. Sun, *Organometallics*, 2011, **30**, 4847–4853.

21 Y. Chen, R. Chen, C. Qian, X. Dong and J. Sun, *Organometallics*, 2003, **22**, 4312–4321.

22 (*a*) C. S. Popeney, A. L. Rheingold and Z. Guan, *Organometallics*, 2009, **28**, 4452–4463; (*b*) Q. Mahmood, Y. Ma, X. Hao and W.-H. Sun, *Appl. Organomet. Chem.*, 2019, **33**, e4857; (*c*) M. Liu, Z. Ning, Y. Ma, G. A. Solan, T. Lian and W.-H. Sun, *J. Organomet. Chem.*, 2023, **994**, 122740; (*d*) Q. Li, S. Liu, Q. Mahmood, Z. Yu, X. Wang, R. Zhang, Y. Wang, G. Ren and W.-H. Sun, *ChemPlusChem*, 2025, e202500315; (*e*) A. Razzaq, Y. Ma, Q. Mahmood, Z. Hu, Y. Wang, S. Zou, A. Zhou, T. Liang, S. Kong and W.-H. Sun, *Eur. J. Inorg. Chem.*, 2024, **27**, e202400380.

23 Z. Wang, G. A. Solan, Q. Mahmood, Q. Liu, Y. Ma, X. Hao and W.-H. Sun, *Organometallics*, 2018, **37**, 380.

24 M. Han, I. I. Oleynik, Y. Ma, I. V. Oleynik, G. A. Solan, X. Hao and W.-H. Sun, *Eur. J. Inorg. Chem.*, 2022, **2022**, e202200224.

25 I. E. Soshnikov, N. V. Semikolenova, A. N. Bushmelev, K. P. Bryliakov, O. Y. Lyakin, C. Redshaw, V. A. Zakharov and E. P. Talsi, *Organometallics*, 2009, **28**, 6003–6013.

26 M. Zada, L. Guo, W. Zhang, Y. Ma, T. Liang and W.-H. Sun, *Eur. J. Inorg. Chem.*, 2021, **2021**, 720–733.

27 M. Han, Q. Zhang, I. I. Oleynik, H. Suo, G. A. Solan, I. V. Oleynik, Y. Ma, T. Liang and W.-H. Sun, *Dalton Trans.*, 2020, **49**, 4774–4784.

28 (*a*) A. S. Abu-Surrah, K. Lappalainen, T. Repo, U. Piironen and M. J. Leskela, *J. Organomet. Chem.*, 2002, **648**, 55; (*b*) C. Huang, S. Du, G. A. Solan, Y. Sun and W.-H. Sun, *Dalton Trans.*, 2017, **46**, 6948–6957.

29 (*a*) G. B. Galland, Ra. Quijada, R. Rojas, G. Bazan and Z. J. A. Komon, *Macromolecules*, 2002, **35**, 339–345; (*b*) E. W. Hansen, R. Blom and O. M. Bade, *Polymer*, 1997, **38**, 4295–4304; (*c*) M. De Pooter, P. B. Smith, K. K. Dohrer, K. F. Bennett, M. D. Meadows, C. G. Smith, H. P. Schouwenaars and R. A. Geerards, *J. Appl. Polym. Sci.*, 1991, **42**, 399–408.

30 N. V. Semikolenova, W.-H. Sun, I. E. Soshnikov, M. A. Matsko, O. V. Kolesova, V. A. Zakharov and K. P. Bryliakov, *ACS Catal.*, 2017, **7**, 2868–2877.

31 L. C. Simon, R. S. Mauler and R. F. De Souza, *J. Polym. Sci., Part A: Polym. Chem.*, 1999, **37**, 4656–4663.

32 P. Giraudeau and E. Baguet, *J. Magn. Reson.*, 2006, **180**, 110–117.

33 Q. Zhang, Z. Li, M. Han, J. Xiang, G. A. Solan, Y. Ma, T. Liang and W.-H. Sun, *Catal. Sci. Technol.*, 2021, **11**, 656–670.

34 (*a*) I. I. Oleinik, I. V. Oleinik, I. B. Abdrakhmanov, S. S. Ivanchev and G. A. Tolstikov, *Russ. J. Gen. Chem.*, 2004, **74**, 1423–1427; (*b*) P. Shaw, A. R. Kennedy and D. J. Nelson, *Dalton Trans.*, 2016, **45**, 11772–11780.

35 O. V. Dolomanov, L. J. Bourhis, R. J. Gildea, J. A. K. Howard and H. Puschmann, *J. Appl. Crystallogr.*, 2009, **42**, 339–341.

36 (*a*) G. M. Sheldrick, *Acta Crystallogr.*, 2015, **71**, 3; (*b*) G. M. Sheldrick, *Acta Crystallogr.*, 2015, **71**, 3.

37 (*a*) R. Zhang, Y. Ma, G. A. Solan, Y. Wang, J. Gao, T. Liang and W.-H. Sun, CCDC 2482813: Experimental Crystal Structure Determination, 2025, DOI: **10.5517/ccdc.csd.cc2pbkrc**; (*b*) R. Zhang, Y. Ma, G. A. Solan, Y. Wang, J. Gao, T. Liang and W.-H. Sun, CCDC 2482814: Experimental Crystal Structure Determination, 2025, DOI: **10.5517/ccdc.csd.cc2pbksd**.